Quantum transport theory for atomic states through solids

D. G. Arbó,[1,2,3] C. O. Reinhold,[1,2] P. Kürpick,[1,2] S. Yoshida,[1,2] and J. Burgdörfer[1,2,4]
[1]*Physics Division, Oak Ridge National Laboratory, Oak Ridge, Tennessee 37831-6373*
[2]*Department of Physics, University of Tennessee, Knoxville, Tennessee 37996-1200*
[3]*Instituto de Astronomía y Física del Espacio, C.C. 67, Succursale 28, 1428 Buenos Aires, Argentina*
[4]*Institute for Theoretical Physics, Vienna University of Technology, A-1040 Vienna, Austria*
(Received 14 January 1999)

We present a quantum description for the evolution of atomic states of fast projectiles traveling through matter. Our approach is based on the solution of a quantum Langevin equation, i.e., a stochastic time-dependent Schrödinger equation that describes electronic excitations of atoms during their transport through solids. The present description can be considered the quantized version of a previously developed classical transport theory. We analyze in detail the correspondence between classical and quantum transport simulations. Applications to the stripping of relativistic H^- and H through thin carbon foils and a comparison with experimental data are presented. [S1050-2947(99)00308-X]

PACS number(s): 34.50.Fa, 34.10.+x

I. INTRODUCTION

Ever since the seminal work by Bohr and Lindhard on the evolution of the charge state and excitation state of fast atomic particles penetrating solids [1], the investigation of the existence and the nature of the electronic excitation spectrum of swift ions has continued to draw considerable interest. A complex array of multiple scattering processes produces a variety of excited configurations not easily accessible by other means. Despite the extensive application of the ion-solid interaction as a spectroscopic tool as well as a ''stripper'' medium to produce high charge states, a microscopic understanding of the dynamics of the excitation process and of the evolution and transport of electrons accompanying fast ions is somewhat limited. The difficulties can be attributed in part to the fact that perturbations of excited states are sufficiently strong to preclude any perturbation treatment.

Some time ago, we proposed a classical transport theory (CTT) [2,3] which is based on a microscopic Langevin equation for the trajectory of projectile-centered electrons. The classical phase-space distribution $\rho_{\rm cl}$ is represented by an ensemble of phase-space points (test particle discretization) whose trajectories are governed by the Langevin equation. Accordingly, the resulting phase-space distribution at a later point in time is determined by the ensemble of evolved phase-space points. In the case that only deterministic fields are present, this approach is equivalent to the classical-trajectory Monte Carlo (CTMC) method [4]. The deterministic force in the Langevin equation contains the Coulomb force between the electron and the projectile nucleus, in general modified by dynamical screening in the solid (''wake'' [5,6]), while the stochastic force represents the random multiple scattering with electrons in the medium (in the simplest case, the ''electron gas'') as well as atomic cores in the target. This prescription has yielded remarkable agreement with a large variety of experimental data, such as for enhanced mean free paths [3], for the enhanced production of high-l Rydberg states and the resulting long-time tail in the delayed x-ray spectra [7], for the yield of convoy yields [8], and, most recently, for the excited state distribution of H(n) at relativistic energies [9,10]. The latter plays a key role for the reference design of next-generation spallation neutron sources (SNSs). An H^- beam in the form of macropulses is accelerated to $\sim$1 GeV in a linear accelerator (LINAC), and is subsequently stripped to bare protons by transmission through a thin foil and injected into and stored in an accumulator ring [11,12]. The effective conversion of H^- to H^+ and the underlying beam-foil interaction at the point of injection is a crucial element for the design of high-intensity SNSs. A key parameter is the population of excited neutrals H(n) which may get stripped by the strong magnetic field in the first bending magnet. The resulting protons collide with walls and magnets leading to unacceptably high levels of radioactivity along the beam line.

Despite the remarkable success of the description of these complex processes within the framework of classical dynamics, the question as to the validity of the CTT has remained open. One particularly puzzling aspect is that a fraction of the collisions suffered by the electron involve small momentum transfers for which classical dynamics is known to break down since excitation and ionization become classically suppressed [13,14]. It appears, therefore, useful to develop a quantum transport approach to gauge the validity and applicability of the classical transport calculations. Until recently, a quantum calculation describing the electronic evolution of an atom as it moves through the solid has appeared to be a formidable task even when the atom carries a single electron. This is due to the fact that a large number of bound and continuum states become populated as a result of the transport process. Only now have a few contributions appeared in the literature in which selected aspects of the ion transmission problem have been tackled by numerically solving the time-dependent Schrödinger equation to calculate resonant coherent excitation rates [15] and stopping of ions [16].

In this work we present a quantum description of transport which is based on a quantum Langevin equation. It describes the stochastic evolution of the quantum state under the influence of both deterministic potentials, specifically a Coulomb potential or a dynamically screened potential, and a stochastic potential which accounts for multiple scattering. The latter is chosen to yield a stochastic force identical to

that entering the classical Langevin equation. In analogy to similar developments in quantum optics [17] and in the theory of atom-radiation-field interaction, each stochastically evolved wave function can be labeled as a ''quantum trajectory'' or ''quantum history.'' The solution of the reduced quantum Liouville equation for the reduced density operator can be reconstructed from a Monte Carlo sampling of quantum trajectories.

Applications to be discussed in the following include the transport of relativistic H^- and H with energies of the order of 1 GeV through carbon foils with applications to the injection problem for spallation neutron sources [11,12] as well as the recent proposal for detecting relativistic antihydrogen [18] through the Ly_α emission after controlled excitation in foil transmission. While the present approach is oriented towards the treatment of the ion-solid interaction, we stress the applicability of this method to a wide variety of other physical situations such as atoms in plasma environments and in the cooler gas of a storage ring or the interaction of atoms with radiation fields.

The plan of this paper is as follows. In Sec. II we give an outline of the theoretical framework. A few technical details of the calculations are presented in Sec. III together with numerical results for H^- transmission. In Sec. IV we focus on the comparison between quantum and classical transport in order to assess the validity of the classical approach and to identify specific quantal, i.e., nonclassical features. Atomic units are used unless otherwise stated.

II. THEORY

We shall be concerned with the transmission of an ion (atom) with nuclear charge Z_p and velocity $\vec{v}_p$ through a thin amorphous foil of thickness X' (we use primes to denote laboratory frame variables). All numerical examples throughout the paper will refer to a carbon foil. However, the method is, with minor modifications, applicable to other materials. The ion, referred to in the following as the projectile, is assumed to be fast compared to the Fermi velocity, v_F, of the material ($v_p \gg v_F$) which corresponds to impact energies greater than hundreds of keV/u. We neglect the slowing down or straggling of the heavy ion due to its interaction with the solid. Typical energy losses for thin foils are a very small fraction of the incident energy and have a negligible effect on the evolution of projectile electrons. Thus, the velocity of the ion is treated as an approximate constant of motion. If desired, the change of the projectile velocity or angular deflection can be easily taken into account, e.g., within the framework of a continuous slowing down approximation (CSDA) and small-angle scattering theory [19,20]. The term transport refers in the following exclusively to the electronic degrees of freedom of the projectile.

We will study the evolution of a single active electron carried by the projectile. For ions carrying more than one electron, additional approximations are required (e.g., see the treatment below for transmission of H^- ions). We decompose this complex system into a subsystem, the atomic state space centered around the projectile taken to be the rest frame, and the environment consisting of atomic cores and the electron gas of the conduction electrons moving at an average velocity of $-\vec{v}_p$. The task is now to determine the evolution of such an open system due to the irregularly fluctuating coupling to the environment, i.e., multiple scattering of the active electron with the constituents of the solid. Since we focus on the transport of electrons which are closely phase space correlated with the projectile, the evolution of the electron in the rest frame of the projectile is governed by nonrelativistic dynamics. Relativistic effects play a role only through the coupling with the environment and its kinematic transformation to the projectile frame.

The state of the electron during the transport process is conveniently described through its density operator

$$\rho = \sum_{j,k} \rho_{j,k} |\phi_j\rangle\langle\phi_k|, \tag{2.1}$$

where $\{|\phi_n\rangle, n=1,2,\ldots,\infty\}$ is a complete orthonormal basis set representing the open subsystem. A density-matrix description easily allows for the treatment of initial electronic states prior to transport which are mixed states,

$$\rho_i = \sum_{\alpha=1}^{N_i} p_\alpha |\alpha\rangle\langle\alpha|, \tag{2.2}$$

where p_α are occupation probabilities of the states $|\alpha\rangle$, or, as a particular case, pure states

$$\rho_i = |\psi_i\rangle\langle\psi_i|, \tag{2.3}$$

where $|\psi_i\rangle$ is the initial wave function. Even though the projectile electron could be in a pure state prior to entering the solid, a random transport process will produce a mixture of states.

The objective of the classical and quantum transport theories is the determination of the time evolution of the state of the electron $\rho(t)$ from $t=0$, prior to entering the solid (or, in general, the time at which the initial state is formed within the solid) up to a time $T = T'\sqrt{1-(v_p/c)^2} = (X'/v_p)\sqrt{1-(v_p/c)^2}$, which corresponds to the foil exit. Our present formulation of quantum transport proceeds by quantization of our classical transport theory (CTT). For reference and comparison, it is therefore useful to first review the major steps of the CTT.

A. Classical Langevin equation

The starting point of the CTT is the time-dependent state of the open system, the active electron, which is given by the reduced probability density $\rho_{\rm cl}(\vec{r},\vec{p},t)$, where $\vec{r}$ and $\vec{p}$ are the position and momentum vectors of the electron. At $t=0$, the probability density is given by

$$\rho_{{\rm cl},i} = \rho_{\rm cl}(\vec{r},\vec{p},0) = \sum_{\alpha=1}^{N_i} p_\alpha \rho_{\rm cl}^\alpha(\vec{r},\vec{p}), \tag{2.4}$$

where $\rho_{\rm cl}^\alpha$ is chosen such that it approximately mimics the quantum state $|\alpha\rangle\langle\alpha|$ (see, e.g., [21]).

The evolution of the open system due to both internal interactions as well as the coupling to its environment (''the bath'') can be described in terms of a reduced classical Liouville equation

$$\frac{\partial \rho_{\rm cl}}{\partial t} = \{\mathcal{H}_{\rm at}, \rho_{\rm cl}\} + \mathcal{R}_{\rm cl}\rho_{\rm cl}$$

$$= -\vec{p}\cdot\vec{\nabla}_{\vec{r}}\rho_{\rm cl} + \boldsymbol{\nabla}_{\vec{r}}\mathcal{V}_{\rm at}\cdot\boldsymbol{\nabla}_{\vec{p}}\rho_{\rm cl} + \mathcal{R}_{\rm cl}\rho_{\rm cl}, \qquad (2.5)$$

where $\{\ ,\ \}$ denote Poisson brackets and $\mathcal{H}_{\rm at}$ is the atomic Hamiltonian

$$\mathcal{H}_{\rm at} = \frac{p^2}{2} + \mathcal{V}_{\rm at}(\vec{r}) = \frac{p^2}{2} - \frac{Z_p}{r} + \mathcal{V}_{\rm scr}(\vec{r}), \qquad (2.6)$$

which contains the Coulomb interaction potential, $-Z_p/r$, possibly modified by dynamical screening (''wake potential'' [5,6]) in the solid, $\mathcal{V}_{\rm scr}$. For the present studies involving low-charged projectiles and very high projectile speeds, $v_p \sim c$, $\mathcal{V}_{\rm at}$ can be approximated by a pure Coulomb potential.

In Eq. (2.5), $\mathcal{R}_{\rm cl}$ is the classical relaxation superoperator describing the dissipative interaction with the environment (the solid). The explicit construction of $\mathcal{R}_{\rm cl}$ is, in general, a formidable task since it involves the many-body dynamics of the environment to which the open system couples. In the present case, $\mathcal{R}_{\rm cl}$ represents the multiple scattering with the solid. The central simplifying assumption which makes the determination of $\mathcal{R}_{\rm cl}$ feasible is the validity of linear-response theory. Accordingly, the dynamics of the bath variables remain decoupled from the internal state $\rho_{\rm cl}$ of the subsystem, or equivalently, $\mathcal{R}_{\rm cl}$ is not of a functional of $\rho_{\rm cl}$. Conversely, no restrictive assumption is made for the strength of the perturbation of the environment on the subsystem. In fact, in the present context we will consider strong coupling that precludes a perturbative treatment of the evolution of the projectile electron under the influence of $\mathcal{R}_{\rm cl}$. In our applications $v_p \gg v_F$ and, therefore, projectile-centered electrons, including those in the continuum, are well separated in momentum space from target electrons. In other words, the removal of an electron from the projectile system is reasonably well-defined and there is little risk of ''double counting.'' Furthermore, we assume that the projectile is fast enough such that collisional interactions with the solid can be represented in terms of impulsive momentum transfers $\vec{q}$. This approximation is based on the observation that collision times $t_c \simeq v_p^{-1}$ are short compared to the orbital period of a hydrogenic electron in a hydrogenic n level, $T_n = 2\pi\omega_n^{-1} = 2\pi n^3 Z_p^{-2}$. With these approximations, the classical relaxation operator is now specified in terms of a collision integral

$$\mathcal{R}_{\rm cl}\rho_{\rm cl} = \int d^3q\, W(\vec{v}_p, \vec{q'})[\rho_{\rm cl}(\vec{r},\vec{p}-\vec{q},t) - \rho_{\rm cl}(\vec{r},\vec{p},t)], \qquad (2.7)$$

where $W(\vec{v}_p, \vec{q'})$ represents the transition rate per unit time to change the electron momentum from $\vec{p'}$ to $\vec{p'}+\vec{q'}$ (see [9] for the transformation of the momentum transfer from the laboratory frame, q', to the projectile frame, q). Equation (2.7) can be viewed as a linearized Boltzmann collision integral. Because of the large separation in momentum space, Pauli blocking does not need to be included. In general, W depends on both the momentum transfer $\vec{q'}$ and the local momentum in the laboratory frame, $\vec{p'}$, as well as on the state of the target which we consider to be in the ground state at zero temperature. For transport of atomic states centered around the projectile with $\langle \vec{p'} \rangle \simeq \vec{v}_p$, we assume that the transition rates are independent of $\vec{p'}$ (i.e., W depends only on $\vec{v}_p$ and $\vec{q'}$). The transition rates are proportional to the differential inverse mean free paths (DIMFPs) or momentum-differential cross sections [22–24] [i.e., $W = v_p(d\lambda^{-1}/d^3q')$, where λ is the mean free path]. They include both elastic and inelastic scattering processes of the active projectile electron with target cores and the electron gas of the medium. The DIMFPs or collision rates are calculated in linear-response theory, which treats the response of the environment, i.e., the electron gas of the medium, due to perturbation by the active electron to first order in the interacting potential but, in general, to all orders of the electron-electron interaction of the medium (e.g., in the random-phase approximation).

Rather than solving Eq. (2.5) directly, the CTT proceeds by employing ''test particle discretization.'' The solution of the original classical Liouville equation for the phase-space density $\rho_{\rm cl}$ is mapped onto the time evolution of a representative ensemble of initial phase points $(\vec{r}_i(0), \vec{p}_i(0))$ chosen by Monte Carlo sampling of the initial probability density,

$$\rho_{\rm cl}(\vec{r},\vec{p},0) = \frac{1}{N_{\rm test}} \sum_{k=1}^{N_{\rm test}} \delta[\vec{r}-\vec{r}_k(0)]\,\delta[\vec{p}-\vec{p}_k(0)], \qquad (2.8)$$

where $N_{\rm test}$ is the number of test particles whose trajectories are determined by a *stochastic* equation of motion, the Langevin equation

$$\frac{d\vec{p}}{dt} = -\nabla_{\vec{r}}\mathcal{V}_{\rm at} + \vec{F}_c(t). \qquad (2.9)$$

Note that the stochastic force F_c describes a discontinuous process representing the momentum ''jumps'' embodied in the collision integral [Eq. (2.7)]. Provided that $\vec{F}_c(t)$ gives a faithful representation of Eq. (2.7), the solution of the original Liouville equation is given by

$$\rho_{\rm cl}(\vec{r},\vec{p},t) = \frac{1}{N_{\rm test}} \sum_{i=1}^{N_{\rm test}} \delta[\vec{r}-\vec{r}_i(t)]\,\delta[\vec{p}-\vec{p}_i(t)]. \qquad (2.10)$$

Since the drift term in Eq. (2.5) agrees with the deterministic part of the Langevin equation (2.9), the only nontrivial part in establishing a correspondence between Eqs. (2.5) and (2.9) lies in the determination of an appropriate stochastic force $\vec{F}_c$. While such a construction is not unique, an obvious strategy is to optimize the agreement with the collision operator for a finite number of jump moments,

$$\frac{d}{dt'}\langle q_i'^n \rangle = \int d^3q'\, q_i'^n W(\vec{v}_p, \vec{q'}) \quad (i=x,y,z), \qquad (2.11)$$

in the absence of $\mathcal{V}_{\rm at}$ (i.e., for free-electron transport).

We use a stochastic force given by a sequence of impulsive momentum transfers (''kicks''),

$$\vec{F}_c = \sum_k \Delta\vec{p}_k\,\delta(t-t_k), \qquad (2.12)$$

where $\Delta\vec{p}_k$ is the stochastic momentum transfer per collision at the time t_k. The determination of $\vec{F}_c(t)$ is thereby reduced to that of a stochastic sequence of pairs $(\Delta\vec{p}_k, t_k)$. The zeroth order of the collision kernel is given by the integrated transition rate $v_p\lambda^{-1}$, where λ is the mean free path between collisions in the laboratory frame. This moment is automatically reproduced by choosing times in between collisions $\Delta t'_k=(t'_k-t'_{k-1})$ at random according to a Poisson distribution

$$\mathcal{P}(\Delta t'_k)\propto\exp[-v_p\Delta t'_k/\lambda]. \tag{2.13}$$

For each collision, the momentum transfer is sampled at random according to a probability density

$$P(\Delta\vec{p'}_k)\propto W(\vec{v}_p,\Delta\vec{p'}_k). \tag{2.14}$$

We have verified that this procedure reproduces up to the second moments of the collision kernels for free-electron transport extremely well [3].

Details of the collision kernels determining the momentum transfers and the times in between collisions have been extensively described elsewhere [3,9,10]. We therefore restrict ourselves to a brief summary. We decompose the stochastic sequence into two independent subsequences. One sequence refers to elastic electron-target core scattering while the other one refers to inelastic electron-electron scattering leading to single-particle–single-hole excitation and to collective excitations of electrons in the medium. Elastic momentum transfers are calculated from the differential elastic cross section for the scattering of electrons at the target cores. Inelastic momentum transfers are obtained from a realistic dielectric function of the foil as a function of the frequency and wave vector [23]. We consider both longitudinal and transverse excitations [5,25]. The main relativistic effect in our calculations is associated with transverse electromagnetic excitations. The mean free path for these excitations decreases for increasing velocity and this process becomes increasingly important at higher collision energies. For carbon foils, however, collisional processes are dominated by longitudinal excitations and elastic scattering. Inelastic longitudinal collisions have the shortest mean free path, while elastic collisions have the largest momentum transfers among the scattering processes.

Our present quantum transport approach consists now of a quantization of the classical transport theory. We start by noting that the classical Langevin equation is completely equivalent to the Hamilton equations of motion associated with the stochastic Hamiltonian

$$\mathcal{H}(t)=\mathcal{H}_{\rm at}+V_c(t)=\mathcal{H}_{\rm at}-\vec{r}\cdot\vec{F}_c(t) \tag{2.15}$$

involving the stochastic potential function $V_c(t)=-\vec{r}\vec{F}_c(t)$ (within the framework of matter-radiation interaction, this corresponds to the so-called length gauge). Here V_c plays the role of a stochastic variable which determines the underlying stochastic process and the relaxation operator.

Moreover, the CTT solution [Eq. (2.10)] generated by this stochastic Hamiltonian is, for transport of a single electron, completely equivalent to the average of various classical solutions each obtained for a particular history or random sequence of collisions $\mu=\{(\Delta\vec{p}_i,t_i),\ i=1,2,\ldots\}$ and for a particular state $|\alpha\rangle\langle\alpha|$ of the initial state mixture. That is,

$$\rho_{\rm cl}(\vec{r},\vec{p},t)=\frac{1}{N_{\rm traj}}\sum_{\alpha=1}^{N_i}p_\alpha\sum_{\mu=1}^{N_{\rm traj}}\rho_{\rm cl}^{\mu,\alpha}(\vec{r},\vec{p},t), \tag{2.16}$$

where $N_{\rm traj}$ is the number of random collisional sequences (ideally, $N_{\rm traj}\to\infty$).

We note a subtle point associated with Eq. (2.16): here we have subjected all $N_{\rm test}$ elements of our classical ensemble to the same stochastic sequence. For a classical ensemble representing a true many-body system, such a choice of stochastic histories would introduce artificial many-body correlations. In the present case, however, the ensemble plays the role of a classical model for the single-particle quantum wave function. Since we will use in the following $\rho_{\rm cl}$ only to calculate one-particle observables, identical stochastic sequences for all members of the ensemble do not affect the numerical results. The present choice is motivated by the direct analogy to the stochastic wave function described in the next section.

B. Quantum Langevin equation

Much like for the classical system, the evolution of an open quantum system can be formally described in terms of a quantum Liouville equation for the reduced density operator ρ of the electron,

$$i\frac{\partial\rho}{\partial t}=[\mathcal{H}_{\rm at},\rho]+\mathcal{R}\rho, \tag{2.17}$$

where the relaxation superoperator $\mathcal{R}$ describes the dissipative interaction with the environment. After making the same simplifying assumptions used in the classical Liouville Eq. (2.5), an explicit, though very cumbersome, form for $\mathcal{R}$ can be given which we omit in the following since we will not directly solve Eq. (2.17). Instead, we solve the quantum transport problem by test-particle discretization of a microscopic quantum Langevin equation, in analogy to the CTT. The stochastic Hamiltonian in Eq. (2.15) generates a stochastic time evolution described by a Schrödinger equation,

$$i\frac{\partial}{\partial t}|\psi(t)\rangle=\mathcal{H}(t)|\psi(t)\rangle, \tag{2.18}$$

to which we refer to in the following as the quantum Langevin equation. Due to the stochastic nature of the Hamiltonian, the time-evolved state $|\psi(t)\rangle$ is indeterministic and Eq. (2.18) is understood to describe a continuous flow in between discontinuous jumps. Each solution $|\psi_{\mu,\alpha}(t)\rangle$ represents one particular realization or history for a given random sequence of collisions, μ, and for a given initial state, $|\alpha\rangle$. While in detail quite different, a solution of the quantum Langevin equation resembles a ''quantum trajectory'' in the terminology of quantum optics [17].

With the help of the quantum Langevin equation, the solution of the transport problem can be easily determined in terms of the Monte Carlo sampling over quantum trajectories or histories, much like the classical solution in Eq. (2.16), i.e.,

$$\rho(t)=\frac{1}{N_{\rm traj}}\sum_{\alpha=1}^{N_i} p_\alpha \sum_{\mu=1}^{N_{\rm traj}} \rho^{\mu,\alpha}(t)$$

$$=\frac{1}{N_{\rm traj}}\sum_{\alpha=1}^{N_i} p_\alpha \sum_{\mu=1}^{N_{\rm traj}} |\psi^{\mu,\alpha}(t)\rangle\langle\psi^{\mu,\alpha}(t)|, \quad (2.19)$$

where, initially, $\psi^{\mu,\alpha}(0)=|\alpha\rangle$.

Using now the explicit form of the stochastic potential in terms of a sequence of impulses [Eq. (2.15)], we can write the solution of the quantum Langevin equation for one particular sequence μ as

$$|\psi^{\mu,\alpha}(T)\rangle=U_\mu(T,0)|\psi(0)\rangle=U_\mu(T,0)|\alpha\rangle, \quad (2.20)$$

where U_μ is the evolution operator after a particular random sequence of collisions $\mu=\{(\Delta\vec{p}_k,t_k),\ k=1,2,\ldots,M\}$. Due to the δ-shaped time dependence of the kicks, the time evolution operator adopts the form

$$U_\mu(T,0)=e^{-i\mathcal{H}_{\rm at}(T-t_M)}\prod_{k=0}^{M-1} U(t_{k+1},t_k), \quad (2.21)$$

$$U(t_{k+1},t_k)=e^{i\vec{r}\cdot\Delta\vec{p}_{k+1}}e^{-i\mathcal{H}_{at}(t_{k+1}-t_k)}, \quad (2.22)$$

where $t_0=0$. That is, in between the times t_k and t_{k+1}, the electron evolves freely according to $\exp[-i\mathcal{H}_{\rm at}(t_{k+1}-t_k)]$. Subsequently, the momentum of the electron is suddenly shifted in $\Delta\vec{p}_{k+1}$, which is exactly described by boost operator $\exp[i\vec{r}\cdot\Delta\vec{p}_{k+1}]$. In practice, upon a basis expansion in terms of atomic (pseudo)states, the operators in the product [Eq. (2.22)] are represented by matrices. Consequently, the calculation of a quantum trajectory is reduced to a sequence of matrix multiplications.

Finally, the time-evolved density operator follows from Eq. (2.19) as

$$\rho(T)=\frac{1}{N_{\rm traj}}\sum_{\alpha=1}^{N_i} p_\alpha \sum_{\mu=1}^{N_{\rm traj}} U_\mu(T,0)|\alpha\rangle\langle\alpha|U_\mu^\dagger(T,0) \quad (2.23)$$

and the expectation value of an arbitrary observable $\mathcal{A}$ is given by $\langle\mathcal{A}\rangle=\mathrm{Tr}(\mathcal{A}\rho(t))$. In particular, for $\mathcal{A}=|\psi_f\rangle\langle\psi_f|$, one obtains the transition probability into a final state $|\psi_f\rangle$ which is given by

$$P_{i\to f}=\frac{1}{N_{\rm traj}}\sum_{\mu=0}^{N_{\rm traj}}\sum_{\alpha=1}^{N_i} p_\alpha|\langle\psi_f|U_\mu(T,0)|\alpha\rangle|^2. \quad (2.24)$$

It is worthwhile noting a few properties of the stochastic evolution operator U_μ. It is obviously not energy conserving within the atomic subsystem since it explicitly treats a time-dependent external perturbation. It therefore allows for energy flow into and out of the ''open'' subsystem in accordance with

$$\frac{d}{dt}\langle\mathcal{H}_{\rm at}\rangle=\frac{d}{dt}\mathrm{Tr}(\mathcal{H}_{\rm at}\rho(t))\neq 0. \quad (2.25)$$

A more subtle feature of U_μ is that any finite-dimensional matrix representation of U_μ, unlike the operator itself, is not unitary. The reason is that both the boost operators $\exp[i\vec{r}\cdot\Delta\vec{p}_k]$ and the free evolution operators $\exp[-i\mathcal{H}_{\rm at}(t_{k+1}-t_k)]$ couple the subsystem to the orthogonal complement Q of any finite-dimensional representation (see the next section). In simple terms, the exact electronic wave function evolves beyond the boundaries of the finite Hilbert space. This loss amounts to a nonunitary evolution with

$$\frac{d}{dt}\ \mathrm{Tr}\rho<0. \quad (2.26)$$

It may appear that the present method depends critically on the choice of the stochastic interaction potential [Eq. (2.15)] in terms of a sequence of δ-shaped pulses. This is, however, not the case. The key observation is that any additional smooth time-dependent potential can be represented in terms of a sequence of infinitesimal kicks as

$$V(t)=\sum_{k=1}^{J}\delta(t-t_k)\,\delta p_k, \quad (2.27)$$

$$\delta p_k=\int_{t_k-\Delta}^{t_k+\Delta} V(t)dt, \quad (2.28)$$

in the limit $\Delta\to 0$, $J\to\infty$, and $T=J\Delta=\mathrm{const}$. The representation of the time-dependent perturbation in terms of a sequence of infinitesimal kicks is just the essence of the so-called split-operator algorithm for integration of the time-dependent Schrödinger equation. Therefore, any combination of deterministic and stochastic time-dependent potentials can be treated according to Eq. (2.22). This includes the effect of external ac and dc fields. The only difference is that for stochastic processes with discrete jumps, the time interval between subsequent kicks, $t_{k+1}-t_k$, remains finite and has physical significance in terms of a characteristic time scale for the stochastic process that determines the interaction between subsystem and environment, while for smooth deterministic processes this interval is to be taken as a finite-difference approximation to a continuous process and is to be made sufficiently small until U_μ is independent of the length of the interval.

Furthermore, Eq. (2.22) permits the treatment of stochastic processes for which the jumps $\Delta\vec{p}(t)$ possess an explicit dependence on time or other parameters. The time-correlation function of the jumps may correspond to ''colored noise'' with long-time correlations. The only restriction is that the stochastic perturbation does not depend on the state of the subsystem. This is in accord with the fundamental assumption of linear response mentioned above.

III. APPLICATIONS

A. Method of calculation

The ultimate purpose of our calculations consists of computing population fractions of various final states after the ion-solid interaction [Eq. (2.24)]. Because typical calculations involve an average over $\gtrsim$1000 trajectories, the key issue for the simulation of the quantum transport is to utilize an efficient and accurate method to numerically evaluate the evolution operator U_μ. The basic pieces for the latter have been developed in a series of recent papers [26,14,27].

An explicit matrix representation of Eq. (2.22) can be found by expanding the wave function in an orthonormal basis set composed of states $|\phi_n\rangle$, $n=1,2,\ldots,N_{\rm max}$,

$$|\psi_\mu(t_{k+1})\rangle = \sum_{s,i,j=1}^{N_{\max}} |\phi_s\rangle\langle\phi_s|e^{i\vec{r}\cdot\Delta\vec{p}_{k+1}}|\phi_i\rangle \times\langle\phi_i|e^{-i\mathcal{H}_{\rm at}(t_{k+1}-t_k)}|\phi_j\rangle\langle\phi_j|\psi_\mu(t_k)\rangle. \tag{3.1}$$

Since the evolution operator couples states of the complete Hilbert space, a finite-dimensional representation of this operator is, in general, not unitary. In other words, if a finite basis set $\{|\phi_n\rangle\}$ is used, the norm of the wave function is not preserved. The amount of probability lost in this nonunitary calculation gives the probability flux to states outside the basis set [see Eq. (2.26)].

Our orthonormal basis set is constructed from a nonorthonormal Sturmian basis set [28–31], which is defined by the complete set of functions obeying

$$\left(\frac{p^2}{2}-\frac{n}{n_s r}\right)|\chi^{n_s}\rangle = -\frac{1}{2n_s^2}|\chi^{n_s}\rangle, \tag{3.2}$$

where $n=1,2,\ldots,\infty$, and the parameter n_s defining the set is called the Sturmian parameter. Equation (3.2) can be solved in spherical coordinates leading to basis states $|\chi^{n_s}_{n,l,m}\rangle$ in terms of spherical quantum numbers. A complete and countable basis set for the full Hilbert space is generated by changing the set of quasi-quantum numbers $n=1,2,\ldots,\infty$, $l=-(n-1),\ldots,(n-1)$, $m=-l,\ldots,l$. In practice, however, the basis must be truncated; i.e., the basis size defined by $N_{\max}$ in Eq. (3.1) is finite. In the following, we use $1\leqslant n\leqslant n_{\max}$, $0\leqslant l\leqslant(n-1)$, $-l\leqslant m\leqslant l$, which corresponds to a number of states $N_{\max}=n_{\max}(n_{\max}+1)(2n_{\max}+1)/6$. By definition, a bound hydrogenic state can be written as $|n,l,m\rangle=|\chi^{n_s}_{n,l,m}\rangle$ if $n_s=n/Z_p$. For hydrogen ($Z_p=1$) the value of n_s determines whether a given n shell is exactly reproduced by the basis (i.e., when $n_s=n$). In general, n_s takes real values and a Sturmian basis set represents a fraction of both bound and continuum energy levels. Understanding which other physical energy levels can be properly described within a finite basis requires additional analysis (see, e.g., [27]).

Since Sturmian functions are not orthogonal, we define the orthonormal basis set $\{|\phi^{n_s}_k\rangle,\ k=1,2,\ldots,N_{\max}\}$ entering Eq. (3.1) as the set of orthonormal eigenvectors of the finite Sturmian representation of $\mathcal{H}_{\rm at}$. Namely,

$$|\phi^{n_s}_k\rangle = \sum_{i=1}^{N_{\max}} b^k_i|\chi^{n_s}_{n_i,l_i,m}\rangle, \tag{3.3}$$

$$\hat{\mathcal{H}}_{\rm at}\hat{b}^k = E_k\hat{S}\hat{b}^k, \tag{3.4}$$

where E_k is the eigenenergy of an electron in the state $|\phi^{n_s}_k\rangle$, $\hat{S}$ is the overlap matrix ($S_{ij}=\langle\chi_{n_i,l_i,m}|\chi_{n_j,l_j,m}\rangle$), and $\hat{b}^k$ and $\hat{\mathcal{H}}_{\rm at}$ are the column vector and matrix representation of $|\phi^{n_s}_k\rangle$ and $\mathcal{H}_{\rm at}$ in the Sturmian basis set, respectively.

Matrix elements of the boost operator, $\exp(i\Delta\vec{p}\cdot\vec{r})$, can be evaluated analytically. First, the matrix elements are calculated in a basis $\chi'_{n,l,m}$ whose quantization axis coincides with the direction of $\Delta\vec{p}$ (see, e.g., [32]). Subsequently, these couplings are rotated for any arbitrary direction $\vec{\Omega}$ of the momentum transfer according to

$$\langle\chi_{n,l,m}|\exp(i\Delta\vec{p}\cdot\vec{r})|\chi_{n',l',m'}\rangle = \sum_{m_1,m_2}\langle\chi_{n,l,m_1}|\exp(i\Delta pz)|\chi_{n',l',m_2}\rangle \times D^l_{m_1 m}(\vec{\Omega})D^{l'}_{m_2 m'}(\vec{\Omega}), \tag{3.5}$$

where $D^j_{m'm}$ are rotation matrix elements.

An accurate nonunitary representation of the free evolution operator in Eq. (3.1), $\exp[-i\mathcal{H}_{at}(t_{k+1}-t_k)]$, requires, in general, a more elaborate treatment such as the use of the complex dilation method [31], masking function, or complex potentials (see, e.g., [33] for a general discussion). In this work we assume that the time in between collision is short enough and that the momentum transfers are large enough such that most of the outgoing flux of probability can be described by the boost operator. Thus, we adopt a unitary matrix representation, $\exp[-i\hat{H}_{\rm at}(t_{k+1}-t_k)]$, within the basis set. Since our basis set diagonalizes $\hat{H}_a$, $\exp(-i\hat{H}_{\rm at}\delta t)$ is also diagonal with matrix elements $\exp(-iE_k\delta t)$ $k=1,2,\ldots,N_{\max}$.

B. Transmission of H^- through thin carbon foils

In order to treat the transport of a two-electron H^- ion, an additional approximation is required which goes beyond the one-electron transport outlined above [9,10]. We reduce the complex problem of $H^-(1s,1s')$-solid interaction to two major steps. First, the weakly bound ''outer'' $1s'$ electron is collisionally detached, thereby leaving the ''inner'' electron in a superposition of states of the H atom. Second, the resulting H atom propagates through the solid experiencing multiple collisions, as described by the present transport approach.

The probability for destruction of H^- as a function of the foil thickness X is given by $P_{H^-}(X')=e^{-X'/\lambda_D}$, where the inverse mean free path (IMFP) for collisional single-electron detachment of H^-, λ_D^{-1}, is approximately given by the total IMFP of free electrons [9]. The sudden collisional removal of the outermost electron leads to a redistribution (shake-up) of the inner electron of H^- among hydrogenic ns states. Using the generalized shake-up approximation and the 20-parameter H^- wave function of Hart and Herzberg [34], it is found that predominantly $H(1s)$ and $H(2s)$ become populated [9]. The probability to find the electron in the $1s$ and $2s$ states is $p_{1s}=0.815$ and $p_{2s}=0.183$, respectively. The population of high ns states including those in the continuum is less than $\approx 0.2\%$. Within this isotropic shake approximation, states of higher angular momenta are not occupied.

The shake-up process creates a coherent excitation of the residual hydrogen atom. However, since the energy and angular distribution of the detached electron remains unresolved, these coherences are partially averaged out. We therefore consider two limiting cases for the initial density matrix. When the phase-space distortion due to the detached electron is strong, we arrive at a completely incoherent state mixture,

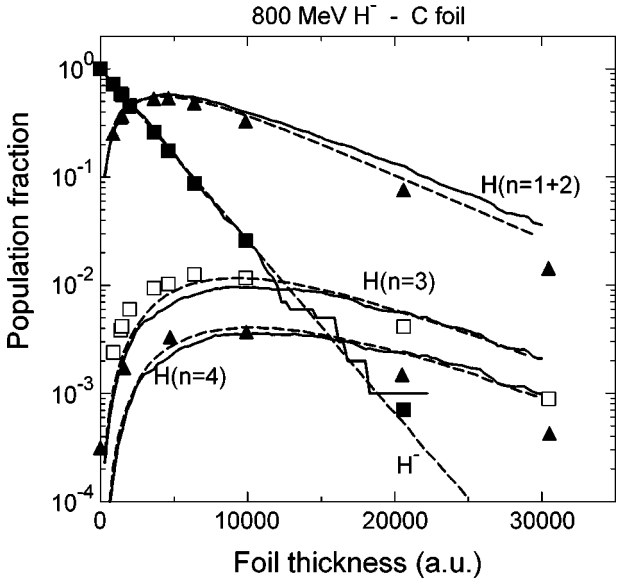

FIG. 1. Fractions of H^- and $H(n=1,2,3,4)$ as a function of foil thickness for transmission of a 0.8 GeV H^- beam through a carbon foil: experimental data of Gulley *et al.* [35] (symbols), quantum transport (solid lines), and classical transport (dashed lines).

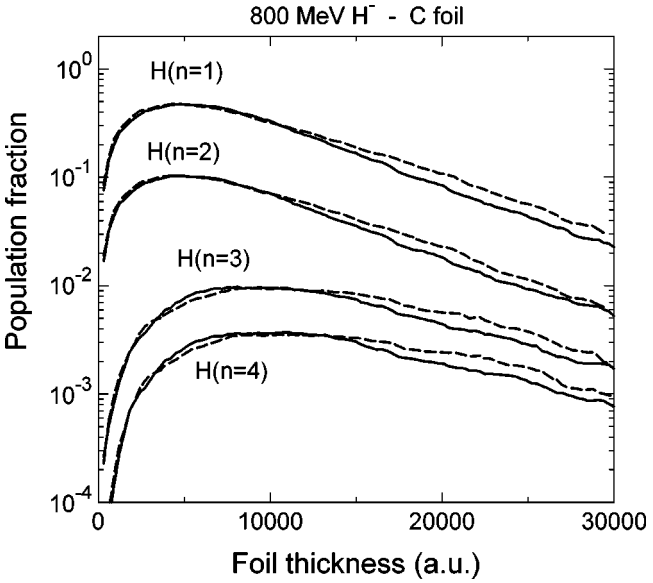

FIG. 2. Illustration of the statistical error of the quantum calculations in Fig. 1. The different calculations have been obtained using two different random sequences of collisions.

$$\rho_i = \sum_n |\psi_{ns}\rangle p_{ns} \langle \psi_{ns}|. \tag{3.6}$$

Conversely, if the residual interaction is negligible (e.g., for an extremely fast receding electron), a pure, fully coherent state

$$\psi_i = \sum_n \sqrt{p_{ns}}\,|\psi_{ns}\rangle \tag{3.7}$$

would result with the relative phases directly given by the shake-up amplitude. We have verified that the numerical results using Eqs. (3.6) and (3.7) agree with each other within our numerical uncertainties. Most of the results presented below are based on Eq. (3.7).

Having generated the initial state after collisional detachment and shake-up, the evolution of the hydrogenic electron in the rest frame of the proton is governed by the nonrelativistic stochastic Hamiltonian [Eq. (2.15)]. Figure 1 illustrates the evolution of outgoing charge state and population fractions of n shells of hydrogen as a function of the foil thickness for a beam energy of 800 MeV. The foil thickness (or time) at which the populations of $H(n=1,2)$ maximize is very different from the ones for $H(n \geqslant 3)$, indicating the existence of different production mechanisms. While shake-up plays a very important role in the population of the $n=1,2$ shells, $n \geqslant 3$ shells are predominantly populated through multiple collisions. An average of eight collisions are involved for the largest foil thickness in the figure. Previous classical transport calculations were found to be in reasonable agreement (within a factor of 2) with experimental data of Gulley *et al.* [35] on an absolute scale (see Fig. 1). We can now test the classical simulation by comparing with our present quantum transport simulation. Remarkably, the quantum and classical calculations are in very good agreement with each other.

Clearly, any firm conclusion from this comparison requires an assessment of the intrinsic errors. Our quantum transport calculations have two sources of errors: statistical and numerical. Statistical errors are associated with the finite number of quantum trajectories involved in the simulation, $N_{\rm traj}=1000$. This is obviously the origin of the fluctuations of the outgoing fraction of H^- ions when the fraction has fallen to below $\approx 10^{-2}$ and which should coincide with the classical result in the limit $N_{\rm traj} \to \infty$. Figure 2 illustrates the statistical error of our calculation of the outgoing fractions of excited states of hydrogen. The two results were obtained using a different ensemble of random collisions and the difference between the curves gives directly a measure for the statistical uncertainties of our results. We therefore estimate the statistical error of our calculations to be $\lesssim 20\%$.

Numerical errors are associated with the truncation effects in the solution of the time-dependent Schrödinger equation in a finite Hilbert space. As a convergence criterion, we use a stabilization method [27] according to which converged results should be stable with respect to variations of our basis size, $N_{\rm max}$, and the Sturmian parameter, n_s. We find that an optimal Sturmian parameter for this problem is $n_s \simeq 3$. Figure 3 illustrates the convergence of our calculations with respect to the basis size as it changes from $N_{\rm max}=140$ ($n_{\rm max}=7$) to $N_{\rm max}=285$ ($n_{\rm max}=9$) states. The relative error of the calculations is found to be $\lesssim 5\%$. The relatively fast convergence is due to the fact that we follow the time evolution only for a relatively short time (about four orbital periods of an $n=2$ electron and about one orbital period of an $n=3$ electron). With increasing time or foil thickness, the error would increase. One physical origin for the breakdown would be the collisional recapture of continuum electrons which becomes a more important process after long periods of time or, equivalently, large distances [8,10]. This would also require a larger basis size to be accounted for accurately.

A more detailed test for the agreement between the classical and quantum simulations is provided by a comparison of the subshell populations of the outgoing hydrogen atoms.

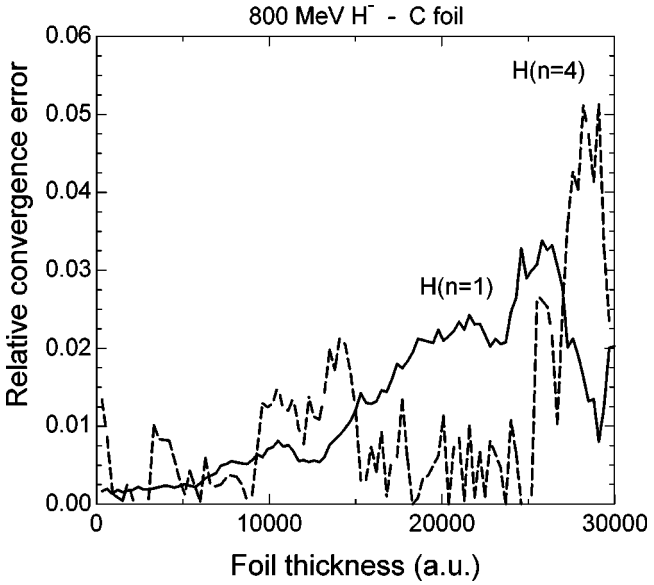

FIG. 3. Relative numerical error of the calculations in Fig. 1 as the basis size is increased from $N_{\max}=140$ ($n_{\max}=7$) to $N_{\max}=285$ ($n_{\max}=9$).

The time-dependent subshell populations of excited hydrogenic states generated during propagation of the hydrogen atom through the foil probe the relative contributions of elastic and inelastic momentum transfer as well as their absolute values and direction and allow for the identification of propensity rules favoring certain quantum numbers. Figure 4(a) displays a comparison between our classical and quantum calculations and the measurements of Keating *et al.* [36] for the m distributions in the $n=4$ shell. Note that the quantization axis is chosen to be perpendicular to the beam velocity $\vec{v}_p$. The agreement between classical and quantum results and the experiment is very good. The $m=0$ population is drastically enhanced compared to a statistical distribution (the statistical weights of $m=0,1,2,3$ are 0.25, 0.375, 0.25, and 0.125, respectively). For small foil thicknesses, the propensity for populating $m=0$ states is primarily driven by the shake-up process following the single-electron detachment of H^-. Remarkably, the preference for populating $m=0$ states extends to all foil thicknesses and, additionally, the population fractions are nearly independent of the foil thickness. This propensity is a consequence of the direction of the typical momentum transfers involved in the transport process: for high-velocity collisions, both elastic and inelastic momentum transfers are nearly perpendicular to the beam axis.

The preferential direction of the momentum transfers also give rise to the propensity to create Stark states whose spatial probability densities have the largest polarization perpendicular to the beam axis. Within each Stark n manifold, the most polarized states correspond to the $m=0$ states. The population fractions of the various $|n,k,m\rangle$ Stark states within a given n manifold obtained theoretically and experimentally [36] are in agreement with this picture. As an example, Fig. 4(b) shows the relative probability within the $n=4$, $m=0$ subshell for populating Stark states with *electric* quantum number $k=-3,-1,1,3$. Both experiment [36] and theory reveal population preferences of the extreme Stark

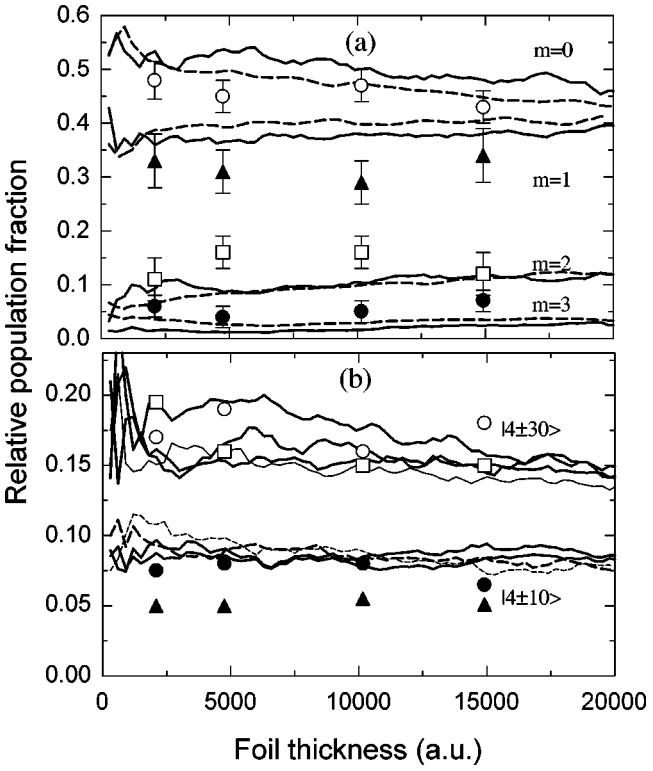

FIG. 4. Substate distributions in the $n=4$ shell as a function of foil thickness for transmission of a 0.8 GeV H^- beam through a carbon foil: experimental data of Keating *et al.* [36] (symbols), quantum transport (solid lines), and classical transport (dashed lines). (a) Relative m distribution. (b) Stark k distribution for $m=0$.

states (large-$|k|$ states) $|4,-3,0\rangle$ and $|4,3,0\rangle$ by about 50% compared to the $|4,-1,0\rangle$ and $|4,1,0\rangle$ states, in accordance with the dominance of transverse momentum transfers. As no strong external magnetic field is present during the transport, the population of states with the same *absolute electric* quantum number should be equal. Small deviations from equal population are a measure of the statistical error of the calculations as well as of the experimental uncertainties.

IV. CORRESPONDENCE BETWEEN CLASSICAL AND QUANTUM TRANSPORT

In order to investigate the origin of the remarkably close classical-quantum correspondence observed for the transport problem in more detail and identify parameter regions where discrepancies might occur, we present in the following results for the evolution of a pure hydrogenic initial state (rather than a mixed state). In addition, we have chosen a collision energy of 8.85 GeV energy which is higher than the one in the preceding section so that the present results can be directly used for recently proposed experiments for the excitation and Ly_α detection of antihydrogen [18]. Note that the same conclusions concerning classical-quantum correspondence are obtained for a beam energy of 0.8 GeV (see, e.g., the scaling properties of the population fractions [10]).

Figures 5 and 6 show that classical and quantum calculations for the n and l distributions of outgoing excited states of hydrogen are again in reasonably good agreement with each other. The main difference with respect to transmission

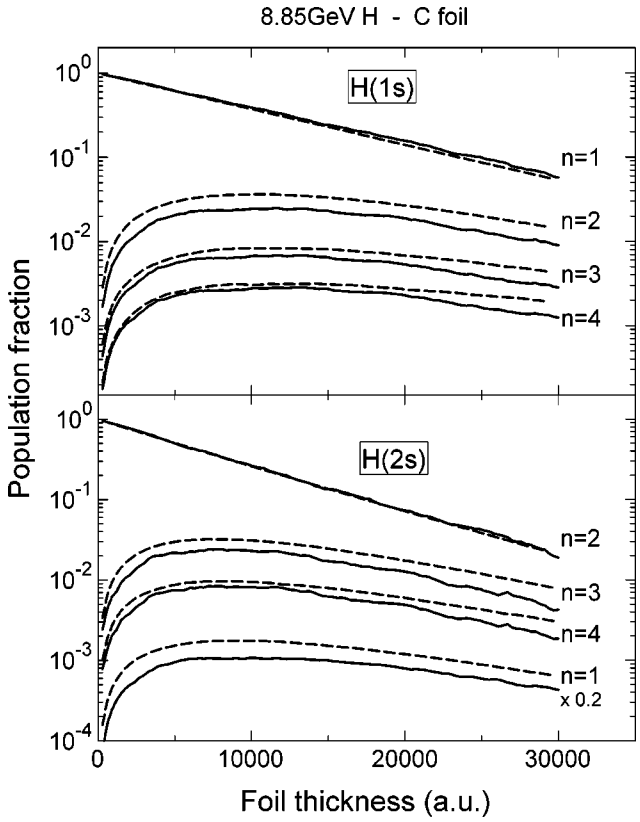

FIG. 5. Fractions of H($n=1,2,3,4$) as a function of foil thickness after transmission of 8.85 GeV H($1s$) and H($2s$) beams through a carbon foil: quantum transport (solid lines) and classical transport (dashed lines).

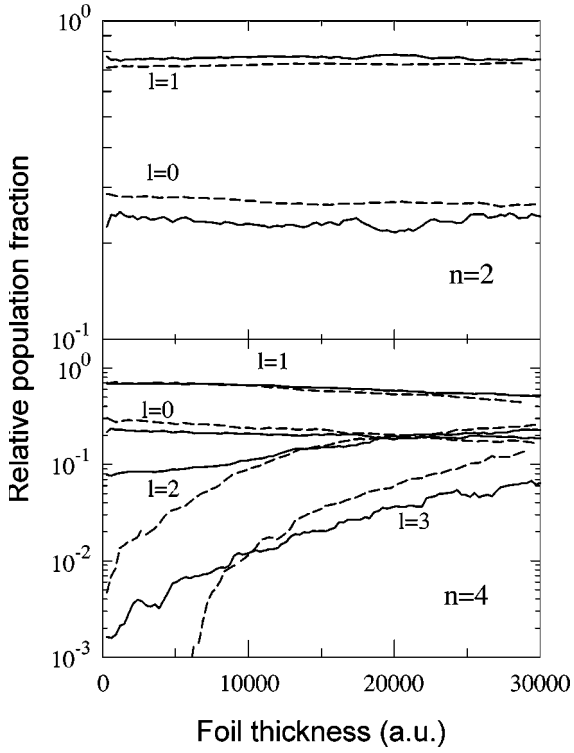

FIG. 6. Substate l distributions in the $n=2$ and $n=4$ shells as a function of foil thickness after transmission of a 8.85 GeV H($1s$) beam through a carbon foil: quantum transport (solid lines) and classical transport (dashed lines).

of H^- is that the fraction of the n level associated with the initial state provides the dominant source of probability and is a monotonically decreasing function of thickness. The dominant angular momentum after excitation from H($1s$) is $l=1$ in accordance with dipole selection rules for soft collisions. The point to be noted is that classical transport can account for the $l=1$ dominance reasonably well despite the fact that dipole transitions due to virtual photon absorption are not properly accounted for within classical dynamics. The biggest differences between the classical and quantum calculations are observed for the population of large angular momentum states at small thicknesses. For increasing foil thickness, the fractions of larger angular momentum states become larger, which is recognized as a signature of multiple scattering (e.g., [37,38,7,39]).

One might expect that the good agreement between classical and quantum transport is due to the benign effect of averaging over many degrees of freedom and parameters (momentum transfers, collision times) inherent in transport. Conversely, the more degrees of freedom are resolved, the better the chances to observe clear discrepancies. Generally speaking, a quantum system reaches its classical limit for short times, strong perturbations, and large quantum numbers. For the transport problem with random flight times in between collisions, however, the Fourier spectrum of the perturbation is broad and, consequently, a time scale for the perturbation can be determined only in terms of an average. This averaging effectively eliminates time coherences which may otherwise lead to, for example, resonant excitation processes. In addition, the transport problem involves an average over the magnitude and the direction of the momentum transfers delivered to the electron.

In order to delineate the origin of the classical-quantum correspondence, we analyze next a simplified problem of an atom subject to a train of impulses (or kicks) for which the randomness of the stochastic force is reduced by keeping the direction and strength constant (i.e., m is a constant of motion),

$$\mathcal{H}_{\rm train}(t)=\mathcal{H}_{\rm at}-z\Delta p\sum_i \delta(t-t_i), \tag{4.1}$$

and by constraining the time interval between collisions, $\Delta t=t_{i+1}-t_i$, to be Poisson distributed, $\mathcal{P}(t_{i+1}) \propto \exp[-(t_{i+1}-t_i)/\langle\Delta t\rangle]$, where the constant $\langle\Delta t\rangle$ represents the average time between collisions. Analysis of this problem can provide evidence as to whether the randomness of the collision times controlled by $\langle\Delta t\rangle$ suffices to achieve the correspondence between the classical and quantum results.

In Fig. 7 we compare classical and quantal ionization of an H($1s$) initial state as a function of Δp after an average number of $N_{\rm kick}=10$ kicks (i.e., $t/\langle\Delta t\rangle=10$), which is a typical number for the transport problem. We display results for two different $\langle\Delta t\rangle$ values, one much smaller and one much larger than the orbital period of the state to be ionized ($T_{\rm orb}=2\pi$ a.u. for $n=1$). As a point of reference, we also show the single kick result for which randomness in time is obviously eliminated. Note that the value $\langle\Delta t\rangle=10\ T_{\rm orb}$ corresponds to the realistic transport calculations discussed above, while $\langle\Delta t\rangle=T_{\rm orb}/10$ corresponds to the ''ultrashort''

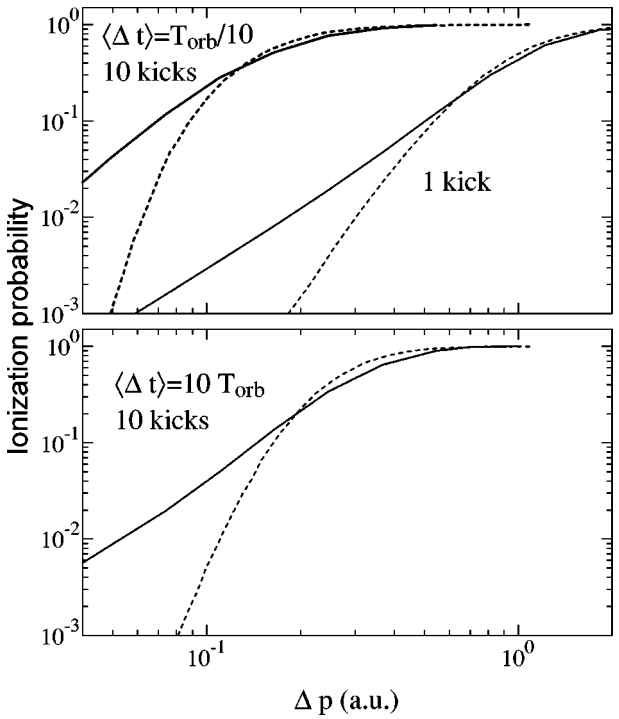

FIG. 7. Ionization probability as a function of the momentum transfer after a H(1s) atom is subject to a single momentum transfer and to a train of constant momentum transfers (kicks) with a random time interval Δt in between them: quantum simulation (solid lines) and classical simulation (dashed lines).

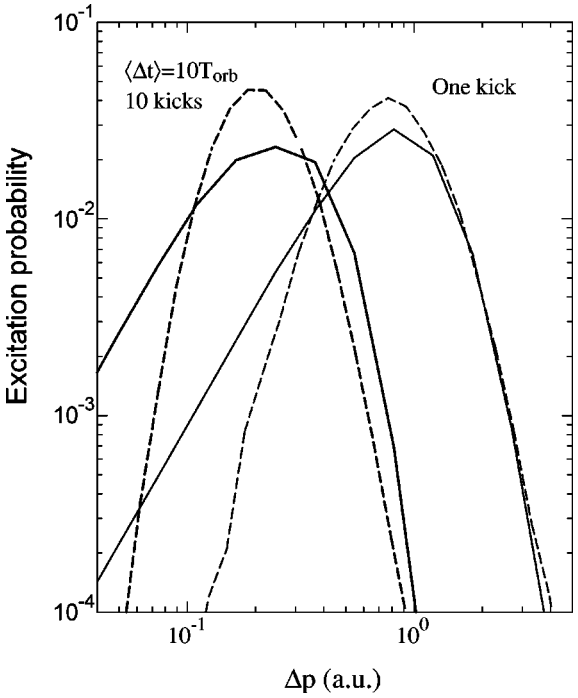

FIG. 8. Excitation probability as a function of the momentum transfer after a H(1s) atom is subject to a single momentum transfer and to a train of constant momentum transfers (kicks) with a random time interval Δt in between them such that $\langle \Delta t \rangle = 10T_{\rm orb}$: quantum simulation (solid lines) and classical simulation (dashed lines).

limit where the time evolution between adjacent kicks can be (almost) neglected and where randomness of collision times should play a minor role.

For a single kick, classical and quantum results are found to be in agreement with each other if the magnitude of the momentum transfer is large enough (e.g., $\Delta p \gtrsim \Delta p_{\rm crit} \approx 0.5$ a.u.). For small momentum transfers, ionization becomes classically suppressed since the classical average energy transferred to the electron $[\langle \Delta E \rangle = (\Delta p)^2/2]$ is much smaller than the level spacing near $n=1$. In turn, the quantum-mechanical result becomes proportional to $(\Delta p)^2$ in the dipole limit (see, e.g., [13,14] for a more detailed discussion). The results after a train of 10 kicks show that the domain of momentum transfers for which classical and quantum results agree shifts to smaller Δp. In the limit $\Delta t \to 0$, this is due to the fact that the sum

$$\Delta \vec{p}_{\rm sum} = \sum_{i=1}^{N_{\rm kick}} \Delta \vec{p}_i \tag{4.2}$$

rather than an individual momentum transfer has to be considered. The effect of 10 collinear kicks becomes exactly equivalent to that of a single kick with ten times larger magnitude. Therefore, $\Delta p_{\rm crit}$ (per kick) above which ionization becomes classical should scale as $1/N_{\rm kick}$, which is approximately observed in Fig. 7. That is, the results for 10 kicks and $\langle \Delta t \rangle = 0.1 T_{\rm orb}$ are shifted in Δp in about a factor of ten with respect to the results for one kick. In turn, for $\langle \Delta t \rangle = 10 T_{\rm orb}$, the relative orientation of $\Delta \vec{p}$ with respect to the local momentum $\vec{p}$ in the orbit between different kicks is randomized. Therefore, one would expect the ''effective'' momentum transfer determining the ionization probability to be $\Delta p_{\rm sum} \simeq \sqrt{N_{\rm kick}} \Delta p$. In this case, the results for 10 kicks should be shifted in $\sim 1/\sqrt{N_{\rm kick}}$ with respect to the results for one kick, which is also approximately observed in Fig. 7.

Figures 8 and 9 show that the conclusions found about classical-quantum correspondence for ionization have to be modified for the excitation probability into the $n=2$ or $n=3$ levels. The excitation probability as a function of the momentum transfer for 10 kicks is shifted compared with the one for a single kick, much like the ionization probability. However, the degree of correspondence after ten random kicks is not as good. Clearly, the excitation probability into a given level is a more delicate case than the total ionization probability, which includes a sum over all continuum energy levels (a more appropriate comparison would be the ionization into a given continuum energy). As expected, the excitation probability is classically suppressed for small momentum transfers. However, depending on the value of $\langle \Delta t \rangle$, the excitation probability for large momentum transfers can be classically suppressed ($\langle \Delta t \rangle = 10$) or enhanced (see [13] for a single kick, which corresponds to the limit $\langle \Delta t \rangle \to 0$). Therefore, not only a lower critical value $\Delta p_{\rm crit}$ above which the classical-quantum correspondence holds has to be considered, but also an upper cutoff exists. In other words, we encounter the following opposing trends: correspondence for excitation into a specific final state exists only for not too large and not too small values of the momentum transfer.

The origin of this apparent puzzle is that classical dynamics can describe the quantum system ''on the average,'' but not all of its peculiarities. In general, classical-quantum discrepancies become larger when the probabilities for the cor-

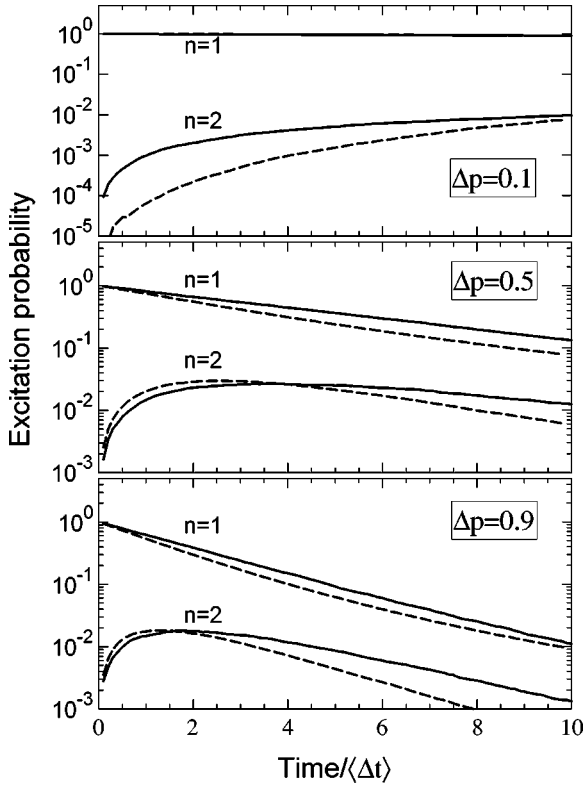

FIG. 9. Fractions of H($n=1,2$) as a function of scaled time after a H($1s$) atom is subject to trains of three different momentum transfers with a random time interval in between them such that $\langle \Delta t \rangle = 10T_{\rm orb}$: quantum simulation (solid lines) and classical simulation (dashed lines).

responding processes become smaller. For a single kick, the bulk of the energy levels that become populated are those whose energy differs from the initial energy in the average energy transfer, $\langle \Delta E \rangle = (\Delta p)^2/2$ (i.e., the so-called Bethe ridge). The probability for excitation into energy levels that are far from this ridge is small and is not properly described by classical dynamics. The breakdown is also visible for many kicks, i.e., in the time evolution of excitation (Fig. 9). As the amount of momentum delivered to the system increases, the classical-quantum discrepancies increase.

Since in addition to the randomness of the collision time also the size of the momentum transfer critically influences the agreement between classical and quantum transport, we can now explore how much randomness in Δp is required to ''repair'' the classical-quantum correspondence and to yield the level of agreement observed in the realistic calculation. To this end, we randomize in our model the values of Δp according to a uniform distribution in the interval $[0.1 \leqslant \Delta p_i \leqslant 1]$ but still keeping the direction fixed. The resulting excitation functions are displayed in Fig. 10 and show that classical and quantum calculations are now in reasonable agreement with each other, the largest deviation for $n=2$ being about 50%. Obviously, as more averaging enters the realistic calculation, the agreement becomes even better.

V. CONCLUSIONS AND OUTLOOK

In this work we have introduced a quantum transport theory to describe the evolution of the excited states of atoms as they are transmitted through the solid. We have presented

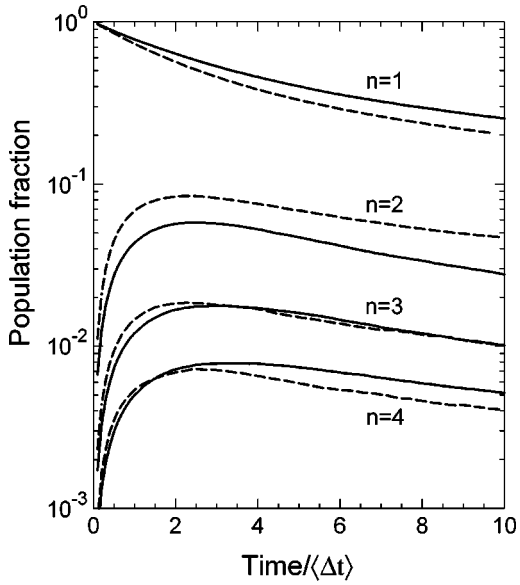

FIG. 10. Fractions of H($n=1,2,3,4$) as a function of scaled time after a H($1s$) atom is subject to trains with random momentum transfers in the interval 0.1 a.u.$<\Delta p<1$ a.u. and with a random time interval in between them such that $\langle \Delta t \rangle = 10T_{\rm orb}$: quantum simulation (solid lines) and classical simulation (dashed lines).

results for the transmission of relativistic H^- and H atoms through thin carbon foils. Our results are found to be in agreement with experiment and classical transport calculations.

We have shown that the surprisingly good agreement between classical and quantum transport is due to two effects. First, the typical momentum transfers in ion-solid collisions are such that they lie, on the average, in the range for which classical-quantum correspondence for a single momentum transfer (''kick'') is expected to exist. Second, the stochastic nature of the collisional interaction destroys quantum effects of time coherence and averages over a broad distribution of momentum transfers.

The present results suggest that promising candidates for which larger discrepancies should appear would be highly charged ions as projectiles. Here, the average collisional energy transfers would be smaller than the quantum level spacings and the critical threshold for classical excitation may not be reached. Thus, the regime of ''small'' nonclassical momentum transfers could be explored. In addition, because of the large value of the projectile charge, dynamical screening and the fine structure of the atom may play an important role. Recent experiments for fast Ar^{18+} and Kr^{36+} ions interacting with carbon foils have found unexplained discrepancies with classical simulations [40]. Work is underway to analyze these systems using the present quantum transport formalism.

ACKNOWLEDGMENTS

Support for this work has been provided by (a) ORNL Director's LDRD Program No. 3211-0846, (b) the U.S. Department of Energy, Office of Basic Energy Sciences, Division of Chemical Sciences, under Contract No. DE-AC05-96OR22464 with ORNL managed by Lockheed Martin Energy Research Corporation, (c) the NSF, and (d) CONICET.

[1] N. Bohr and L. Lindhard, K. Dan. Vidensk. Selsk. Mat. Fys. Medd. **26**, 12 (1954).
[2] J. Burgdörfer, in *Proceedings of the Third Workshop on High Energy Ion-Atom Collisions,* Vol. 294 of Lecture Notes in Physics, edited by D. Berenyi and G. Hock (Springer-Verlag, Berlin, 1988), p. 344.
[3] J. Burgdörfer and J. Gibbons, Phys. Rev. A **42**, 1206 (1990).
[4] R. Abrines and I. C. Percival, Proc. Phys. Soc. London **88**, 861 (1966); **88**, 873 (1966); I. C. Percival and D. Richards, Adv. At. Mol. Phys. **11**, 1 (1975).
[5] J. Neufeld and R. Ritchie, Phys. Rev. **98**, 1632 (1955); **99**, 1125 (1955).
[6] P. Echenique, W. Brandt, and R. H. Ritchie, Phys. Rev. B **33**, 43 (1979).
[7] J. Burgdörfer and C. Bottcher, Phys. Rev. Lett. **61**, 2917 (1988); J. Kemmler, J. Burgdörfer, and C. O. Reinhold, Phys. Rev. A **44**, 2993 (1991).
[8] C. O. Reinhold, J. Burgdörfer, J. Kemmler, and P. Koschar, Phys. Rev. A **45**, R2655 (1992).
[9] B. Gervais, C. Reinhold, and J. Burgdörfer, Phys. Rev. A **53**, 3189 (1996).
[10] P. Kürpick, C. O. Reinhold, J. Burgdörfer, and B. Gervais, Phys. Rev. A **58**, 2183 (1998); C. O. Reinhold, P. Kürpick, J. Burgdörfer, and S. Yoshida, Nucl. Instrum. Methods Phys. Res. B **146**, 76 (1998).
[11] The NSNS Collaboration, National Spallation Neutron Source Conceptual Design Report, Oak Ridge National Laboratory Report No. NSNS/CDR-2, 1997 (unpublished).
[12] *Outline Design of the European Spallation Neutron Source,* edited by I.S.K. Gardner, H. Lengeler, and G. H. Rees, 1995 (unpublished).
[13] C. O. Reinhold and J. Burgdörfer, J. Phys. B **26**, 3101 (1993).
[14] C. O. Reinhold, M. Melles, H. Shao, and J. Burgdörfer, J. Phys. B **26**, L659 (1993); **29**, 377 (1996).
[15] F. J. Garcia de Abajo and P. M. Echenique, Phys. Rev. Lett. **76**, 1856 (1996).
[16] G. Schiwietz and P. L. Grande, Radiat. Eff. Defects Solids **130**, 137 (1994).
[17] M. O. Scully and M. S. Zubairy, in *Quantum Optics* (Cambridge University Press, New York, 1995).
[18] G. Blanford, K. Gollwitzer, M. Mandelkern, J. Schultz, G. Takei, G. Zioulas, D. C. Christian, and C. T. Munger, Phys. Rev. D **57**, 6649 (1998).
[19] L. Landau, J. Phys. (Moscow) **8**, 1 (1944).
[20] S. Goudsmit and J. L. Saunderson, Phys. Rev. **57**, 24 (1940).
[21] R. Becker and A. MacKellar, J. Phys. B **17**, 3923 (1984); J. Pascale, C. O. Reinhold, and R. E. Olson, Phys. Rev. A **42**, 5305 (1990); C. O. Reinhold and C. A. Falcón, *ibid.* **33**, 3859 (1986).
[22] P. Sigmund and K. Winterbon, Nucl. Instrum. Methods **119**, 541 (1974); S. Tougard and P. Sigmund, Phys. Rev. B **25**, 4452 (1982).
[23] J. Ashley, C. Tung, and R. Ritchie, Surf. Sci. **81**, 409 (1979); C. Martin, E. Arakawa, T. Callcott, and J. Ashley, J. Electron Spectrosc. Relat. Phenom. **35**, 307 (1985); J. Ashley, J. Cowan, R. Ritchie, V. E. Anderson, and J. Hoelzel, Thin Solid Films **60**, 361 (1979); J. Ashley, J. Electron Spectrosc. Relat. Phenom. **28**, 177 (1982).
[24] C. Tung, Surf. Interface Anal. **11**, 69 (1986).
[25] U. Fano, Annu. Rev. Nucl. Sci. **13**, 19 (1963).
[26] M. Melles, C. O. Reinhold, and J. Burgdörfer, Nucl. Instrum. Methods Phys. Res. B **79**, 109 (1993).
[27] S. Yoshida, C. O. Reinhold, J. Burgdörfer, B. E. Tannian, R. A. Popple, and F. B. Dunning, Phys. Rev. A **58**, 2229 (1998).
[28] M. Rotenberg, Ann. Phys. (N.Y.) **19**, 262 (1962); Adv. At. Mol. Phys. **6**, 233 (1970).
[29] R. Shakeshaft, Phys. Rev. A **18**, 1930 (1978); **14**, 1626 (1976).
[30] M. Pont, D. Proulx, and R. Shakeshaft, Phys. Rev. A **44**, 4486 (1991).
[31] A. Maquet, S. Chu, and W. P. Reinhart, Phys. Rev. A **27**, 2946 (1983).
[32] Dž Belkić, J. Phys. B **14**, 1907 (1981); the basic integrals can be actually found in, e.g., I. G. Gradshteyn and I. M. Ryshik, in *Table of Integrals, Series, and Products* (Academic Press, San Diego, 1980), p. 844.
[33] S. Yoshida, S. Watanabe, C. O. Reinhold, and J. Burgdörfer, Phys. Rev. A **60**, 1113 (1999).
[34] J. F. Hart and G. Herzberg, Phys. Rev. **106**, 79 (1957).
[35] M. S. Gulley, P. B. Keating, H. C. Bryant, E. P. MacKerrow, W. A. Miller, D. C. Rislove, S. Cohen, J. B. Donahue, D. H. Fitzgerald, S. C. Frankle, D. J. Funk, R. L. Hutson, R. J. Macek, M. A. Plum, N. G. Stanciu, O. B. van Dyck, and C. A. Wilkinson, Phys. Rev. A **53**, 3201 (1996).
[36] P. B. Keating, M. S. Gulley, H. C. Bryant, E. P. MacKerrow, W. A. Miller, D. C. Rislove, S. Cohen, J. B. Donahue, D. H. Fitzgerald, D. J. Funk, S. C. Frankle, R. L. Hutson, R. J. Macek, M. A. Plum, N. G. Stanciu, O. B. van Dyck, and C. A. Wilkinson, Phys. Rev. A **58**, 4526 (1998).
[37] Y. Yamazaki *et al.*, Phys. Rev. Lett. **61**, 2913 (1988).
[38] J. P. Gibbons *et al.*, Phys. Rev. Lett. **67**, 481 (1991).
[39] P. Nicolai, M. Chabot, J. P. Rozet, M. F. Politis, A. Chetioui, C. Stephan, A. Touati, D. Vernhet, and K. Wohrer, J. Phys. B **23**, 3609 (1990).
[40] D. Vernhet, J. P. Rozet, E. Lamour, B. Gervais, C. Fourment, and L. J. Dube, Phys. Scr. (to be published); D. Vernhet, J. P. Rozet, I. Bailly-Despiney, C. Stephan, A. Casimi, J-P. Grandin, and L. J. Dube, J. Phys. B **31**, 117 (1998); E. Lamour, Ph.D. thesis, Universite de Caen, 1997 (unpublished).